J. Geophys. 40, 189–202, 1974

Long Range Propagation of Seismic Energy in the Lower Lithosphere*

R. Kind

Geophysikalisches Institut der Universität Karlsruhe

Received December 10, 1973

Abstract. Observations of seismic arrivals from the lower lithosphere in France revealed a low mean velocity of observed first arrivals of about 8.1 km/s between 150 and more than 1000 km distance and several high velocity phases with apparent velocities between about 8.2 and 8.6 km/s. Each one of these high velocity phases is only observed over a range of about 100 or 200 km. The possibility of interpreting these phenomena in terms of fine structure of the lower lithosphere is investigated. The resulting model consists of alternating high and low velocity layers. No first order discontinuities seem to exist between these layers. A reliable quantitative estimate of the thickness of these high and low velocity zones can only be obtained by a joint travel time and amplitude study.

Key words: Long Range Profiles — Deep Seismic Sounding — Synthetic Upper Mantle Seismograms.

Introduction

Hirn, Steinmetz, Kind and Fuchs (1973) have presented data, and an interpretation of a long range seismic profile in France. Hereafter this paper will be referred to as paper I. The observed seismogram section in Fig. 1 is reproduced from paper I for a more convenient comparison with the results of the present paper. The same phase labels are used as in paper I. The interpretation of the observed data was attempted in paper I in terms of fine structure of the lower lithosphere by a joint inversion of travel times and amplitudes (see appendix for a comment on the travel time fit of the proposed model in paper I). This kind of interpretation was confirmed by Hirn (1973) for the phase labelled P_I. He used several seismic profiles from bore hole shots of high frequency content to evaluate the regional extension of the structure, which causes this phase. Supplementary experiments were

---

* Contribution Nr. 166 within the research program "Unternehmen Erdmantel" of the Deutsche Forschungsgemeinschaft.

Contribution Nr. 101, Geophysikalisches Institut der Universität Karlsruhe.

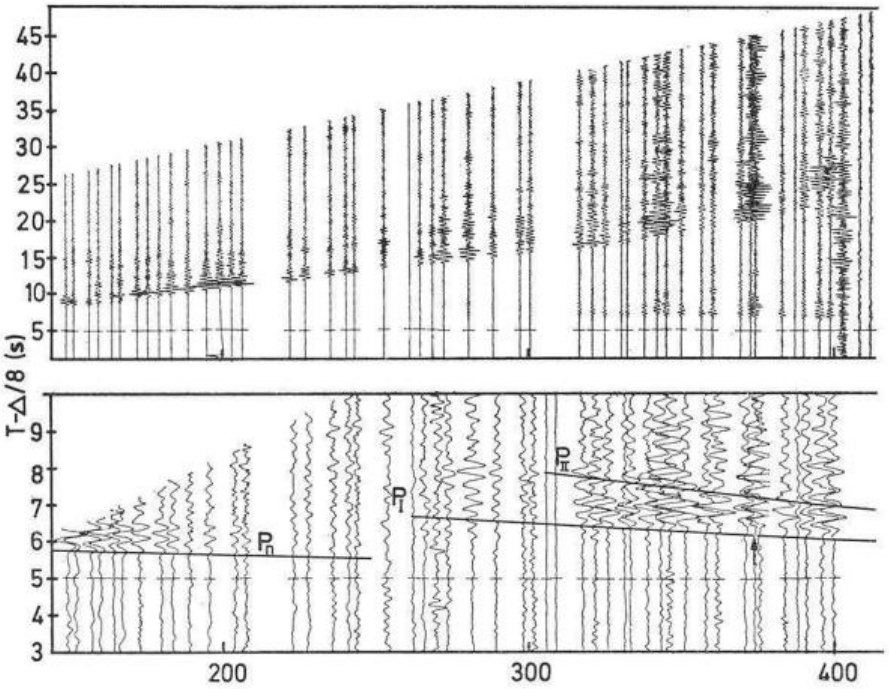

Fig. 1. Seismogram section from a long range profile from Brest to Toulon in France (Hirn *et al.*, 1973). Top: Low time resolution, low amplification record section. Bottom: High time resolution, high amplification record section. The travel time curves of the model in Fig. 12 and Table 1 are superimposed on the record section. Critical points are marked by arrows

carried out in the summer of 1973 to confirm the existence of the phase labelled P_{II}. A preliminary interpretation of these experiments seems to confirm the structure which causes this phase. These experiments however also revealed that the amplitudes of this phase vary considerably with azimuth (Groupe Grands Profils Sismiques (France), German Research Group for Explosion Seismology, Swiss Deep Seismic Sounding Group, 1973).

The most important features of the observed seismogram section, which must be reproduced by any resulting model, should be repeated here. They are a low mean velocity of the observed first arrivals of about 8.1 km/s between 150 and more than 1000 km distance, and several high velocity phases with apparent velocities between about 8.2 and 8.6 km/s. Each one of these high velocity phases, which are labelled P_I, P_{II} and P_{III}, is only observed over a range of about 100 or 200 km distance. A very similar

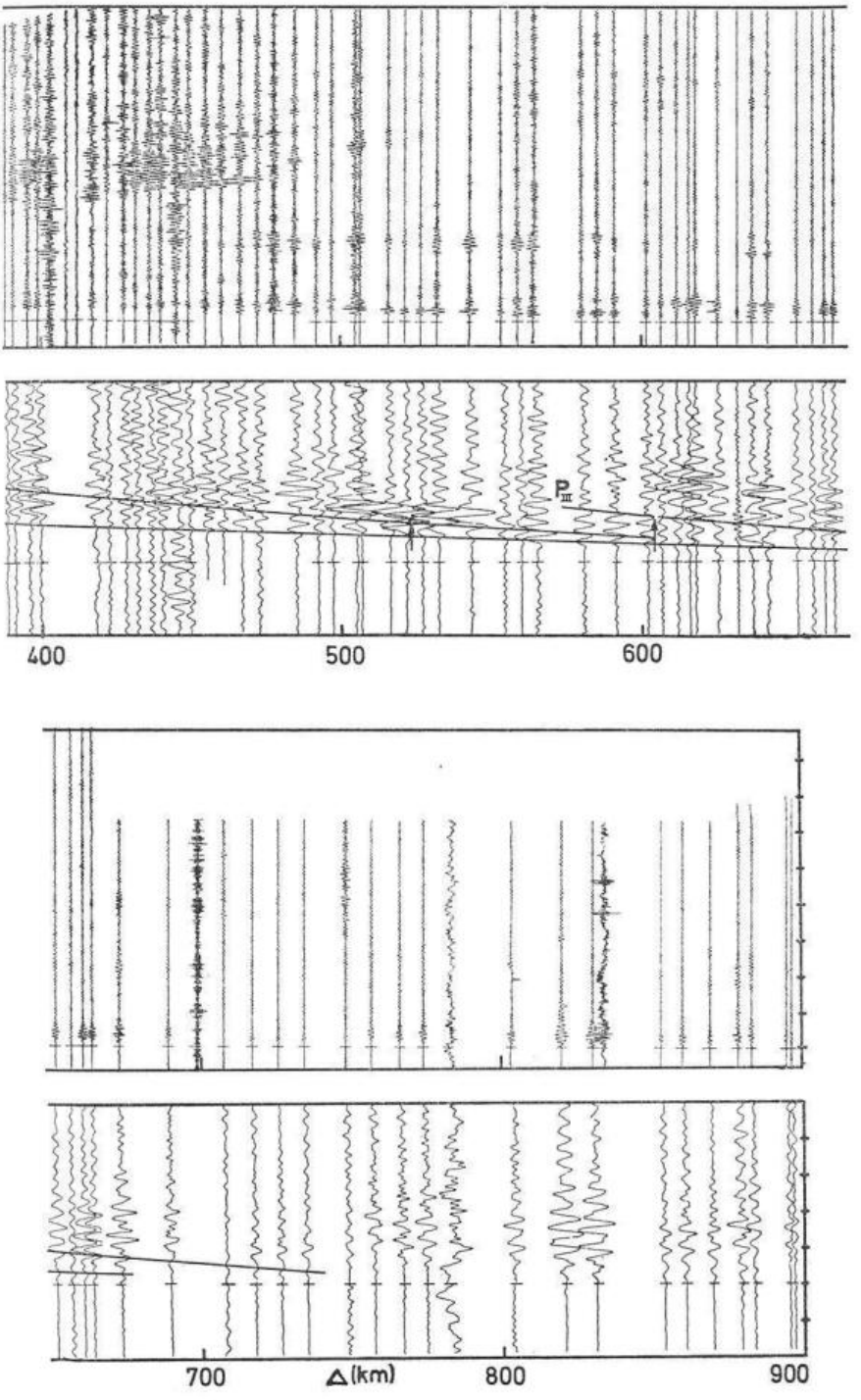
P_m
400
500
600
700
Δ(km)
800
900

picture is observed on several long range profiles in different parts of the world. Ryaboi (1966) reports it south of Lake Aral, and it is also observed on Early Rise profiles in south-westerly and westerly direction (Massé, 1973). On the Canadian Shield, however, the observed high velocity phases do not stop but continue over much longer distances (Massé, 1973). The same seems to be true in oceanic areas (Hales *et al.*, 1970). The proposed model in paper I consists of a low velocity zone beneath the Moho, followed by a 8.2 km/s layer and a 8.45 km/s half space. Although this type of model is consistent with travel time and amplitude observations up to 600 or 700 km distance, it fails to model the low mean velocity of first arrivals at larger distances. The synthetic seismograms, on which the amplitude interpretation is based, have too much energy beyond 700 km distance at too early arrival times. The solution of this problem is the subject of the present paper. It will also be attempted to explain a possible third phase, labelled P_{III} in Fig. 1, in terms of fine structure of the lower lithosphere, although this phase is not yet confirmed by additional field experiments. The purpose of the present paper is not to prove the existence of fine structure in the lower lithosphere, since this can only be done by a sufficient number of field experiments. It can only be attempted here to investigate by numerical experiments, if there are possibilities at all to reproduce the observed phenomena under the assumption of vertical variation of velocity alone.

Method

Besides the inversion of travel times, the interpretation method is based on synthetic seismograms. The method for the computation of synthetic seismograms, and the assumption on which it is based, are described by Fuchs and Müller (1971). The most severe limitation for the present purpose is the assumption of lateral homogeneity. Synthetic seismograms will be computed for models with increasing complexity from Fig. 2 to Fig. 12. The starting model is a simple crust mantle model and more details will be added in each figure in an attempt to fit the observed phenomena. The following remarks are valid for all computed seismogram sections. The P velocity depth function is plotted in each figure. Poisson's ratio is assumed to be $^1/_4$, the density is obtained from Birch's law (density $=$ $0.252 + 0.3788 \cdot$ P velocity). Different values of the density or Poisson's ratio are not discussed in the present paper. The curvature of the earth is approximately taken into account (Müller, 1971). The source signal used for the numerical calculations has a cosine spectrum with zeros at 0.0 and 4.5 Hz. The frequency increment is 0.05 Hz. In order to save computer time the reflected wave field was only computed within a phase velocity

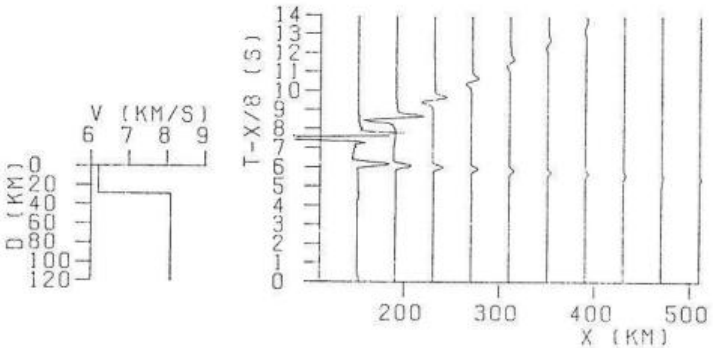

Fig. 2. Synthetic seismograms of the P velocity model at the left side of the figure. The P_n head wave can be followed up to 500 km

window between 6.6 and 10.0 km/s. Therefore only these phases or parts of phases with velocities within this window can be recognized in the computed sections. When a phase approaches one of these boundary velocities, as does the Moho reflection in all figures, then a rapidly decaying phase with this boundary velocity arises from the calculations. This is due to a purely numerical effect. The angle increment in the interval between the angles of incidence, corresponding to the boundary velocities, is 0.07 degrees. The vertical component of the P wave response is plotted. All seismograms are plotted on the same scale.

Results

In Fig. 2 synthetic seismograms for a simple crust mantle model are shown. The Moho reflection and the head wave are already separated at the shortest distance plotted. The important point in this figure is, that the P_n wave for this model has detectable energy up to more than 500 km distance. However, the observed P_n wave stops early, at about 200 km. In Fig. 3 the 8.1 km/s half space is replaced by a 9 km thick 8.1 km/s layer, which is followed by a 7.9 km/s half space. Now the head wave travelling in the lid stops at much shorter distances. Although the geometrical ray theory does not predict a head wave travelling in the 7.9 km/s half space of the model in Fig. 2, a very weak 7.9 km/s long period head wave is detectable in Fig. 2. This is due to the leaking of the long period components of the input pulse through the high velocity lid. The P_n head wave is followed in time by a reflection from the discontinuity at the bottom of the lid. In Fig. 4 an 8.2 km/s half space is placed below the low velocity layer of the model of Fig. 3. This structure reflects energy in the distance range between

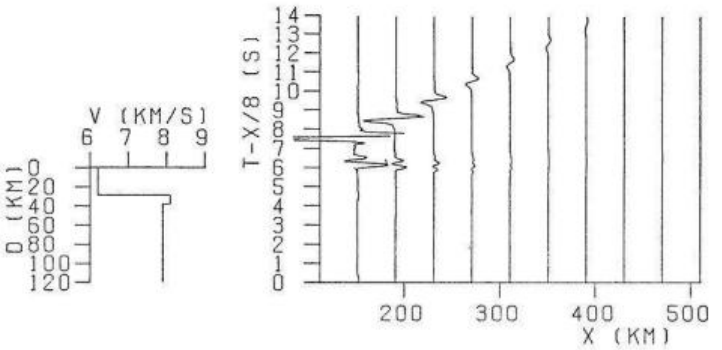

Fig. 3. The 8.1 km/s half space of the model in Fig. 2 is replaced by a 7.9 km/s half space 9 km beneath the crust mantle boundary. P_n stops at a much shorter distance. A reflection from the bottom of the lid follows P_n in time

about 200 and 400 km, whereas the main energy of the observed P_I phase is concentrated between about 300 and 400 km distance. A head wave travelling in the half space can be followed up to 700 or 800 km distance, which is not in agreement with the observed data. Two internal multiple reflections within the channel can be recognized at larger distances as later arrivals. In Fig. 5 the first order discontinuities are replaced by gradients. The main effect is the concentration of the energy of P_I in the desired range between 300 and 400 km. In addition the reflection from the lower boundary of the lid is strongly reduced. The head wave in the half space has larger amplitudes. In Fig. 6 a low velocity half space of 3.0 km/s is placed below the 8.2 km/s layer. Only a high velocity lid is left. The lower boundary of this lid is a first order discontinuity. Such a model causes the 8.2 km/s head wave to disappear. It also reduces the amplitudes of the reflection from the high velocity zone mainly at larger distances. However, too large amplitudes are introduced between 200 and 300 km. They result from a reflection from the first order discontinuity at the bottom of the high velocity lid. In Fig. 7 this first order discontinuity is replaced by a gradient, thus reducing these amplitudes. The last few figures have shown, that a high velocity zone, like the one in Fig. 7, is able to model a high velocity phase, which is only observed over a limited distance range. The thickness of the high velocity zone relative to the dominant wavelength of the input signal is important. It was found that the upper limit of the thickness is of the order of magnitude of the dominant wavelength. If one increases the thickness too much, then the head wave travels too far and the mean velocity of the observed first arrivals is becoming too high. In Fig. 8 the thickness of the high velocity zone is reduced to 2 km, which is about half the dominant wavelength. This

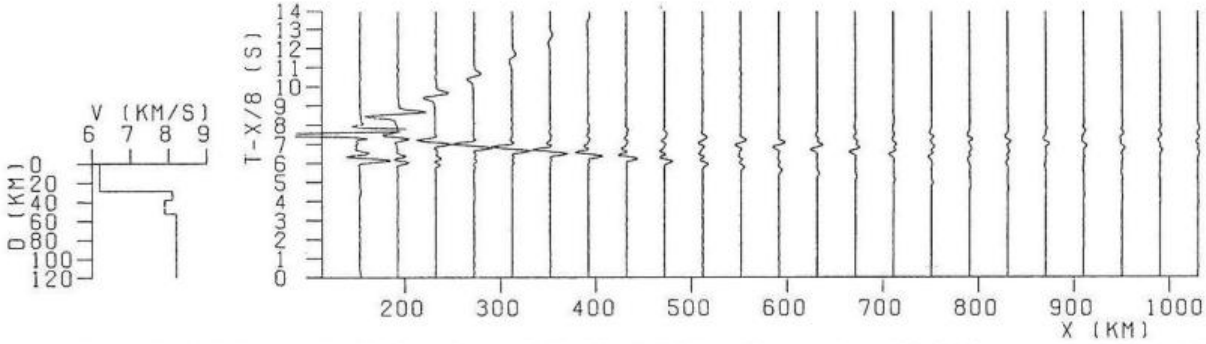

Fig. 4. An 8.2 km/s half space is added to the model in Fig. 3. Reflected energy from this half space appears between 200 and 400 km. Several multiples within the channel can be recognized. The 8.2 km/s head wave can be followed up to 800 km distance

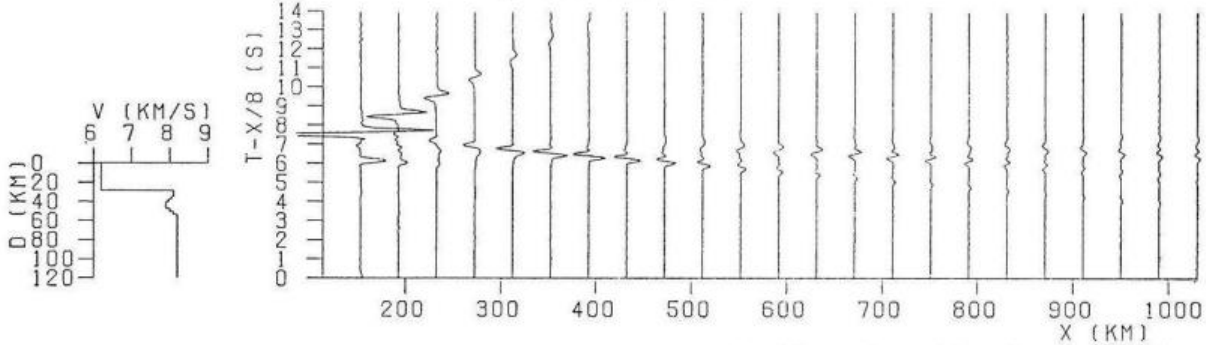

Fig. 5. The first order discontinuities of the model in Fig. 4 are replaced by gradients. The reflected energy from the half space is concentrated between 200 and 300 km distance. The 8.2 km/s head wave has more energy than the comparable head wave in Fig. 4

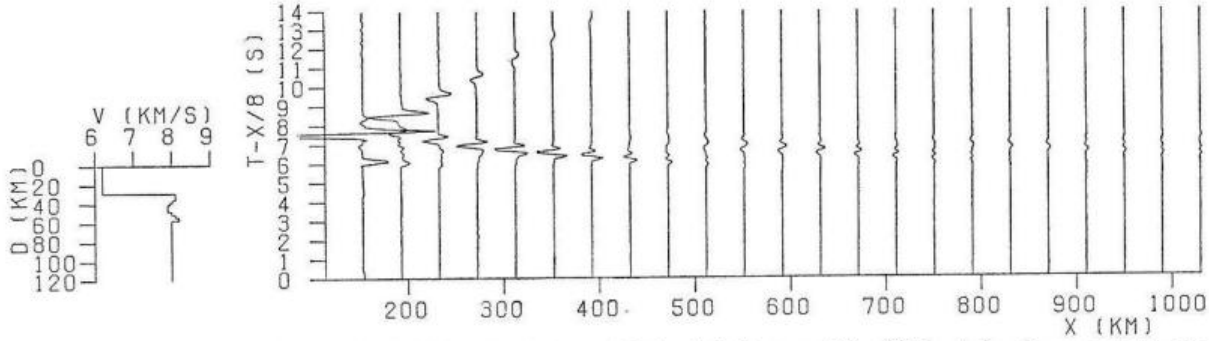

Fig. 6. The 8.2 km/s half space of Fig. 5 is replaced by an 8.0 km/s half space. The 8.2 km/s head wave stops at a much shorter distance, which keeps the mean velocity of first arrivals low. Reflected energy from the first order discontinuity at the bottom of the 8.2 km/s lid appears between 200 and 300 km distance

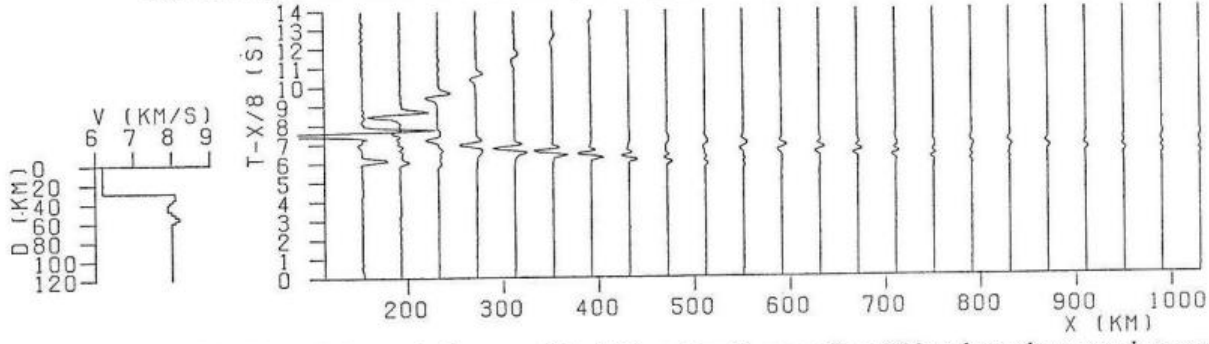

Fig. 7. The first order discontinuity at the bottom of the lid is replaced by a gradient. This reduces the energy between 200 and 300 km. This model reproduces the phases P_n and P_I

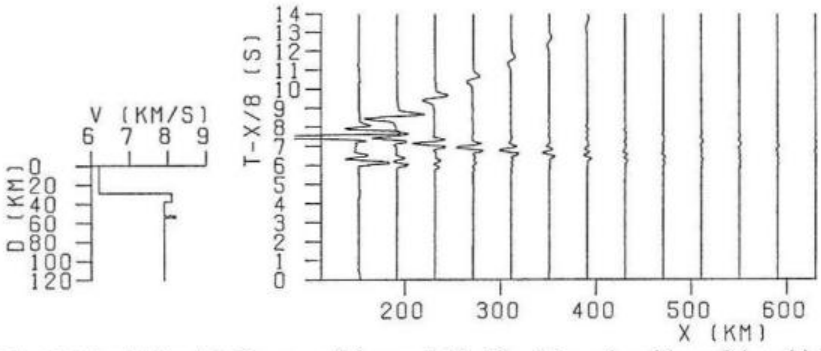

Fig. 8. The 8.2 km/s half space of the model in Fig. 4 is replaced by a 2 km thick layer, which is about half the wave length of the input signal. The reflected energy from this very thin high velocity zone is still comparable with the energy reflected from the half space. The main energy is, however, shifted towards undercritical distances

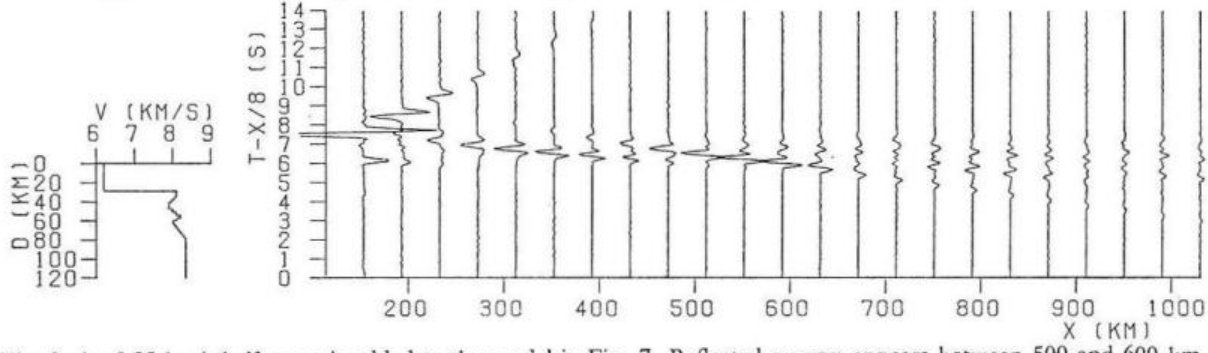

Fig. 9. An 8.35 km/s half space is added to the model in Fig. 7. Reflected energy appears between 500 and 600 km. The head wave in the half space can be followed up to 1000 km

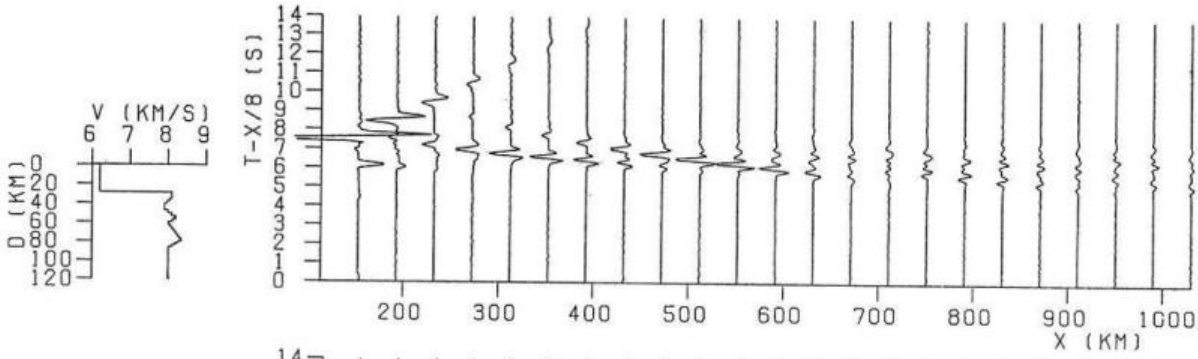

Fig. 10.

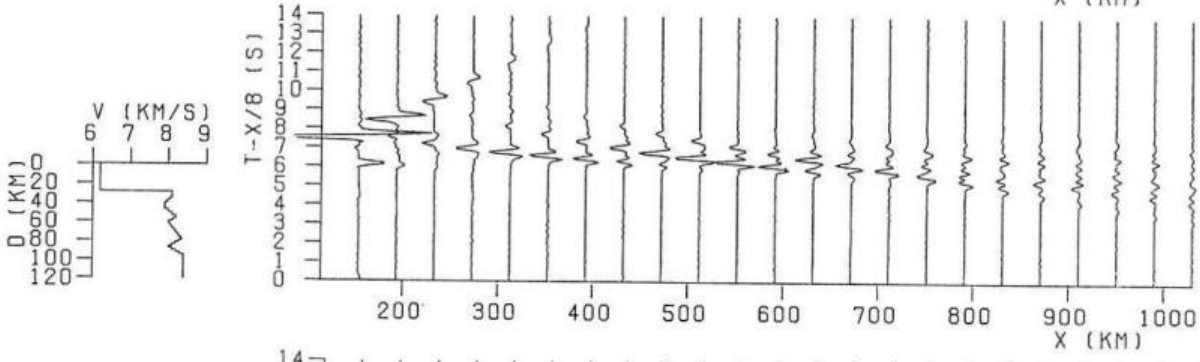

Fig. 11.

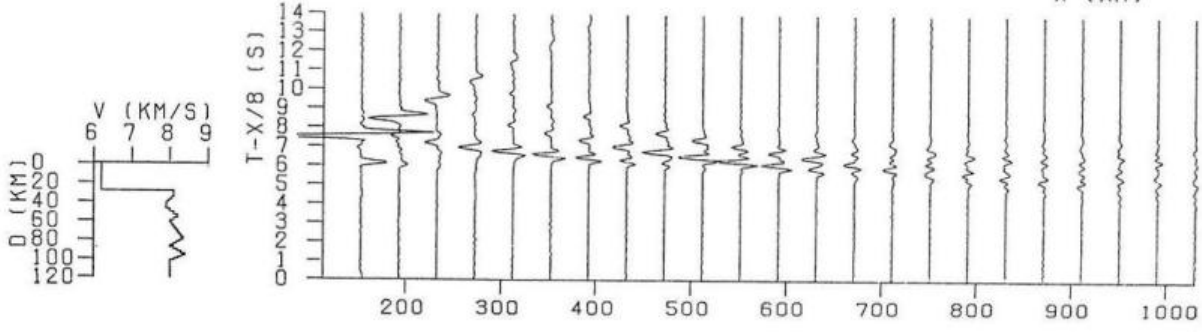

Fig. 12.

figure shows that the energy reflected from top and bottom of this very thin high velocity zone is still comparable in size with the energy reflected from the half space in Fig. 4. However, the energy is much more shifted towards undercritical distances.

The inversion of the P_{II} and P_{III} phases in Fig. 1 was carried out along the same lines as for P_I. The P_{II} phase is modelled in Fig. 9 and Fig. 10. The mean velocity of the first arrivals in Fig. 10 is very similar to the observed one. This requirement was violated by the model in paper I. It should be noted that the entire energy beyond about 700 km in Fig. 10 is due to internal multiples only. Although the P_{III} phase is the least clear one and a more energetic source could improve the data, it was attempted in Fig. 11 and Fig. 12 to model this phase by the same method. In Fig. 11 the requirement of low mean velocity of first arrivals does not seem to be fulfilled at the end of the profile. Therefore, the high velocity half space is replaced by a low velocity one in Fig. 12. This reduces the mean velocity of first arrivals. The energy at undercritical distances, however, is increased due to a reflection

Table 1. P velocity depth distribution of the model in Fig. 12

depth (km)	P-velocity (km/s)
0.	6.2
29.	6.2
29.	8.1
35.5	8.1
40.5	7.9
47.5	7.9
57.5	8.2
62.5	8.0
80.	8.35
88.	8.0
97.	8.4
102.	8.0

←

Fig. 10. The 8.35 km/s half space is replaced by an 8.0 km/s half space, which causes the 8.35 km/s head wave to disappear and keeps the mean velocity of first arrivals low. This model reproduces the phases P_n, P_I and P_{II}

Fig. 11. An 8.4 km/s half space is added to the model in Fig. 10. Reflected energy appears between about 600 and 700 km and the 8.4 km/s head wave can be recognized up to 1000 km

Fig. 12. The 8.4 km/s half space is replaced by an 8.0 km/s half space. This keeps the mean velocity of first arrivals low, but it increases the energy in undercritical distances. This model reproduces the phases P_n, P_I, P_{II} and parts of P_{III}

from the negative gradient. The numerical values of the model in Fig. 12 are shown in Table 1. The travel time curves of this model are plotted in Fig. 1. The travel time curve of the P_n wave is the only one corresponding to a true head wave. The travel time curves of all other phases are formed by overcritical and undercritical reflections. The travel time fit of the P_{III} phase in the distance range between about 580 and 620 km is not as satisfying as it is in larger distances. The observed apparent velocity reaches between about 580 and 620 km values of about 10 km/s. It seems to be likely that lateral variations are the cause of this observation. Therefore, the attempt to fit the P_{III} phase with the assumption of lateral homogeneity was only partially successful. If this phase is caused by a high velocity zone in about 100 km depth, as indicated in Fig. 12, then this zone is probably laterally disturbed.

Conclusions

The most important features of the observed section in Fig. 1, which are low mean velocity of first arrivals and several high velocity phases, are modelled in Fig. 12 with sufficient accuracy. The agreement is very good for the P_n, P_I and P_{II} phases and could be somewhat better for the P_{III} phase. This result indicates, that there are possibilities to interpret most of the features of the observed data in terms of fine structure of a horizontally stratified lower lithosphere down to about 100 km depth, even with the assumption of lateral homogeneity. The remarkable point of the resulting model is, that it consists of several alternating high and low velocity zones. An amplitude study is definitely required for a reliable quantitative estimate of the model parameters. The results of the present paper seem to support ideas about the existence of high velocity layers in the lower lithosphere as suggested by Kosminskaya *et al.* (1972) and in paper I. The preferred thickness of the high velocity zones is around 4 km, which is about the dominant wavelength of the input signal. However, measurable effects from high velocity layers much thinner than the length of an input wave should be obtained. This can be seen from Fig. 8. This figure also indicates, that a great danger of erroneous interpretation exists in the case of reflections from local, nonhorizontal, thin high velocity zones. This emphasizes the importance of a sufficient number of experiments, which are available in the case of the P_n and P_I phases and perhaps of the P_{II} phase but not yet in the case of the P_{III} phase. Gradients instead of first order discontinuities are a very powerful tool for shaping the amplitude distance curves of reflected waves. It seems to be difficult to achieve with the assumptions outlined in the description of the method a similar degree of agreement using first order discontinuities only, as was suggested in the upper mantle

models of Ansorge and Müller (1973) and Mayer-Rosa and Müller (1973). All the energy in the computed section of Fig. 12 beyond about 800 km distance is due to internal multiple reflections. Therefore, any correlation of phases in this distance range without enough data at shorter ranges could lead to erroneous interpretations.

Appendix

The arrival times of the P_I and P_{II} phases of the model presented in paper I are too late relative to the observed arrival times. The time delay is between about 0.5 and 0.8 s. This occurred due to an erroneous determination of the onset time of the input pulse in the synthetic seismograms. A correction of this error does not influence the general results of paper I. This statement is made in agreement with all the authors of paper I.

Acknowledgement. This research was made possible by a grant of the Deutsche Forschungsgemeinschaft. I wish to thank Dr. Gerhard Müller and Prof. Dr. Karl Fuchs for many stimulating discussions and for reading the manuscript. Dr. Lee Alsop also read the manuscript and Ingrid Hörnchen typed it. The extensive computations were carried out at the computer center of the University of Karlsruhe.

References

Ansorge, J., Müller, St.: The P-wave structure of the uppermost mantle in Europe based on long range explosion observations. Z. Geophys. *39*, 385–394, 1973

Fuchs, K., Müller, G.: Computation of synthetic seismograms with the reflectivity method and comparison with observations. Geophys. J.R.A.S. *23*, 417–433, 1971

Groupe Grands Profils Sismiques (France), German Research Group for Explosion Seismology, Swiss Deep-Seismic Souding Group: Lateral variations in the structure of the lower lithosphere in France. Paper presented at the first Meeting of the European Geophysical Society. Zürich, 1973

Hales, A.L., Helsley, D.E., Nation, J.B.: P traveltimes for an oceanic path. J. Geophys. Res. *75*, 7362–7381, 1970

Hirn, A.: Data on the lower lithosphere from recent seismic profiles in France. Paper presented at the first Meeting of the European Geophysical Society. Zürich, 1973

Hirn, A., Steinmetz, L., Kind, R., Fuchs, K.: Long range profiles in Western Europe: II. Fine structure of the lower lithosphere in France (southern Bretagne). Z. Geophys. *39*, 363–384, 1973

Kosminskaya, I.P., Puzyrev, N.N., Alekseyev, A.S.: Explosion seismology: its past, present and future. In: A. R. Ritsema (ed.), The upper mantle. Tectonophysics *13*, 309–323, 1972

Massé, R.P.: Compressional velocity distribution beneath central and eastern North America. Bull. Seism. Soc. Am. *63*, 911–935, 1973

Mayer-Rosa, D., Müller, St.: The gross velocity-depth distribution of P- and S-waves in the upper mantle of Europe from earthquake observations. Z. Geophys. *39*, 395–410, 1973

Müller, G.: Approximate treatment of elastic body waves in media with spherical symmetry. Geophys. J. R.A.S. *23*, 435–449, 1971

Ryaboi, V.Z.: Kinematic and dynamic characteristics of deep waves associated with boundaries in the crust and upper mantle. Izv. (Bull.) Acad. Sci. USSR, Geophys. Ser., AGU Transl., *3*, 177–184, 1966

Dr. Rainer Kind
Geophysikalisches Institut
D-7500 Karlsruhe 21
Hertzstraße 16
Federal Republic of Germany